Front. Phys. 13(6), 132105 (2018)
https://doi.org/10.1007/s11467-018-0829-4

REVIEW ARTICLE

Lattice quantum chromodynamics and baryon-baryon interactions

Tetsuo Hatsuda

RIKEN Interdisciplinary Theoretical and Mathematical Sciences Program (iTHEMS), Wako, Saitama 351-0198, Japan
Corresponding author. E-mail: thatsuda@riken.jp
Received July 9, 2018; accepted July 30, 2018

After briefly reviewing the theoretical concepts and numerical methods in lattice QCD, recent simulation results of the hadron masses and hadron interactions with nearly physical quark masses are presented. Special emphasis is placed on the baryon-baryon interactions on the basis of the HAL QCD method where the integro-differential equation for the equal-time Nambu–Bethe–Salpeter amplitude plays a key role to bridge a gap between the multi-baryon correlation and the scattering observable such as the phase shift.

Keywords lattice QCD, nuclear force, exotic hadron

PACS numbers 11.15.Ha, 12.38.Gc, 13.75.Cs, 12.39.Mk

Contents

1 Introduction

Lattice quantum chromodynamics (LQCD) allows first-principle, gauge invariant and non-perturbative calculations of strongly interacting quarks and gluons [1]. In the past 40 years, LQCD simulations have been extensively applied to study heavy quark potentials, hadron masses, hadronic matrix elements, QCD phase transition at finite temperature, and so on [2]. In recent years, there are also progresses in deriving the baryon-baryon interactions [3], which are particularly relevant to nuclear physics and astrophysics.

*Special Topic: Simplicity, Symmetry, and Beauty of Atomic Nuclei (Eds. Jie Meng, Takaharu Otsuka & Yu-Min Zhao).

The functional integral representation of the the Euclidean QCD partition function $\mathcal{Z}$ on a finite spatial box L^3 and the temperature T is given by $\mathcal{Z}(T,V,J) = \int [\mathrm{d}A\mathrm{d}\bar{q}\mathrm{d}q] \exp(-\int_0^{1/T} \mathrm{d}\tau \int_{L^3} \mathrm{d}^3x \, (\mathcal{L}^{\mathrm{E}}_{\mathrm{QCD}} + J\Xi)$ where the Euclidean QCD Lagrangian in terms of quarks q^α and gluons A^b_μ is given by

$$\mathcal{L}^{\mathrm{E}}_{\mathrm{QCD}} = \bar{q}^\alpha (\Gamma_\mu D^{\alpha\beta}_\mu + m\delta^{\alpha\beta}) q^\beta + \frac{1}{4} G^b_{\mu\nu} G^b_{\mu\nu}, \tag{1}$$

The quark mass matrix in the flavor space $(u, d, s, \cdots)$ is denoted by m with the flavor indices suppressed. The color covariant derivative is defined by $D^{\alpha\beta}_\mu = \partial_\mu \delta^{\alpha\beta} + \mathrm{i}g A^{\alpha\beta}_\mu$, with $x_\mu = (\tau, \boldsymbol{x})$, $\partial_\mu = (\partial_\tau, \nabla)$ and the 3×3 matrix field, $A_\mu = A^b_\mu t^b$. The field strength tensor is $G_{\mu\nu} = G^b_{\mu\nu} t^b$ with $G^b_{\mu\nu} = \partial_\mu A^b_\nu - \partial_\nu A^b_\mu - g f_{bcd} A^c_\mu A^d_\nu$. The arbitrary external fields (such as the external source of the quarks and gluons, external electroweak fields etc) are denoted by J, with the corresponding dynamical operators $\Xi(A, \bar{q}, q)$. The functional integration measure for gluons and quarks is defined by $[\mathrm{d}A\mathrm{d}\bar{q}\mathrm{d}q] \equiv \prod_{x,\mathrm{color},\mathrm{spin},\mathrm{flavor}} \mathrm{d}A^b_\mu(x) \mathrm{d}\bar{q}^\alpha(x) \mathrm{d}q^\beta(x)$. The temporal boundary condition of the gluon (quark) field is periodic (anti-periodic); $A^b_\mu(\tau = 0, \boldsymbol{x}) = A^b_\mu(\tau = 1/T, \boldsymbol{x})$, $\bar{q}^\alpha(\tau = 0, \boldsymbol{x}) = -\bar{q}^\alpha(\tau = 1/T, \boldsymbol{x})$, and $q^\beta(\tau = 0, \boldsymbol{x}) = -q^\beta(\tau = 1/T, \boldsymbol{x})$. The spatial boundary conditions are not constrained and can be taken to be either periodic or anti-periodic; the difference should disappear in the thermodynamic limit, $L \to \infty$. To calculate low-energy hadron properties below 1 GeV, we need to evaluate the functional integral with full quantum fluctuations. The

lattice QCD provides a way to carry out such task numerically in a gauge invariant manner.

In this article, we first review the theoretical concepts and numerical methods of lattice QCD in Chap. 2, 3 and 4 on the basis of Ref. [4]. Then, we will discuss some of the recent results of baryon-baryon interactions on the lattice at nearly physical point (the pion mass is about 146 MeV) with large spacetime volume $(8.1\ \mathrm{fm})^4$ on the basis of Refs. [5, 6].

2 Lattice QCD: Theoretical concepts

Let us first start with the Wilson line which is defined on a path P connecting the point y and x in the continuous Euclidean spacetime. By parametrizing the path in terms of a coordinate $z(s)$ with $z(s=0)=y$ and $z(s=1)=x$, the Wilson line reads $U_P(x,y;A)=\mathrm{P}\ \exp\left(\mathrm{i}g\int_0^1 \mathrm{d}s\lambda_\mu A_\mu\right)$ with $\lambda_\mu=\mathrm{d}z_\mu/\mathrm{d}s$. The path ordered symbol P is introduced, since $A_\mu=A_\mu^b t^b$ is a matrix in the color space. The Wilson line has the following properties: (i) $U_P(x,y;A)=U_{P_2}(x,z(s);A)U_{P_1}(z(s),y;A)$, (ii) $\frac{\mathrm{d}}{\mathrm{d}s}U_P(z(s),y;A)=[\mathrm{i}g\lambda(s)\cdot A(z(s))]\,U_P(z(s),y;A)$, and (iii) $U_P(x,y;A)\to U_P(x,y;A^V)=V(x)U_P(x,y;A)V^\dagger(y)$ under local gauge transformation. The gauge-invariant quark bilinear $\bar q(x)U_P(x,y;A)q(y)$, and the gauge-invariant Wilson loop $\mathrm{tr}\ U_P(x,x;A)$ turn out to be important building blocks to define the QCD on the lattice.

Consider a four dimensional hyper-cubic lattice with a lattice spacing a and the four dimensional volume L^4. Each lattice site is specified by n_μ corresponding to the Euclidean coordinates through $x_\mu=an_\mu$. The link variable is a special unitary matrix connecting the neighboring sites n and $n+\hat\mu$, $U_\mu(n)=\exp(\mathrm{i}gaA_\mu(n))$. Here $\hat\mu$ implies a vector pointing the direction of μ with a length a. Also, any non-minimal Wilson line on the lattice is represented by a product of link-variables. For later purpose, we introduce a link variable pointing the opposite direction as $U_{-\mu}(n+\hat\mu)=[U_\mu(n)]^\dagger$. The smallest closed loop can be defined as $U_{\mu\nu}(n)=U_\nu^\dagger(n)U_\mu^\dagger(n+\hat\nu)U_\nu(n+\hat\mu)U_\mu(n)$. Under local gauge transformation, $U_\mu(n)\to V(n)U_\mu(n)V^\dagger(n+\hat\mu)$, it transforms as $U_{\mu\nu}(n)\to U_{\mu\nu}^V(n)=V(n)U_{\mu\nu}(n)V^\dagger(n)$.

In the continuum limit ($a\to 0$), we have $\mathrm{tr}(U_{\mu\nu}(n)-1)=-\frac{1}{4}g^2a^4(G_{\mu\nu}^b(n))^2+O(a^5)$. Therefore, a gluon action on the lattice, which reduces to the Yang-Mills action in the leading order, reads

$$S_\mathrm{G}=\beta\sum_\mathrm{Pl}\left[1-\frac{1}{N_c}\mathrm{Re\ tr}\ U_{\mu\nu}(n)\right]$$
$$=\frac{1}{g^2}\sum_n\sum_{\mu\neq\nu}\mathrm{tr}\,[1-U_{\mu\nu}(n)]\xrightarrow{a\to 0}\frac{1}{4}\int\mathrm{d}^4x G_{\mu\nu}^b(x)^2, \tag{2}$$

where $\sum_\mathrm{Pl}$ is a sum over all non-oriented plaquettes (minimum square tile on the lattice with the area a^2). Note that $\beta\equiv 2N_c/g^2$ with N_c being the number of colors ($N_c=3$ for QCD). The lattice gluon action is not unique in the sense that one may add arbitrary non-minimal terms which vanish in the continuum limit.

There exist three types of gauge invariant objects made of nearest neighbor fermions, $\bar q(n)q(n)$, $\bar q(n+\hat\mu)U_\mu(n)q(n)$, and $\bar q(n-\hat\mu)U_{-\mu}(n)q(n)$. Here one may put any γ-matrices between $\bar q$ and q without spoiling the color gauge invariance. A special combination of the above terms is called the Wilson's fermion action

$$S_\mathrm{F}\equiv a^4\sum_{n',n}\bar q(n')(m\delta_{n',n}+D_\mathrm{W}(n',n;U))q(n)$$
$$\xrightarrow[a\to 0]{}\int\mathrm{d}^4x\bar q(x)\left(\Gamma_\mu D_\mu+m-\frac{ar}{2}D_\mu^2\right)q(x), \tag{3}$$

where the Wilson's Dirac operator with the Wilson's parameter r reads

$$D_\mathrm{W}(n',n;U)=-\frac{1}{2a}\sum_{\pm\mu}[\delta_{n',n+\hat\mu}(r+\Gamma_\mu)U_\mu(n)-r\delta_{n',n}]\,. \tag{4}$$

Here the Euclidean Dirac matrices are defined as $\Gamma_\mu\equiv(\gamma_4=\gamma^0,-\mathrm{i}\boldsymbol{\gamma})$, $\Gamma_{-\mu}\equiv-\Gamma_\mu$, and $\Gamma_5\equiv\gamma^5$, so that they satisfy the relations, $\{\Gamma_\mu,\Gamma_\nu\}=2\delta_{\mu\nu}$ and $\Gamma_\mu^\dagger=\Gamma_\mu$ with $\mu=1,2,3,4,5$. One of the important properties of $D_\mathrm{W}(n',n;U)$ is its Γ_5 Hermiticity, $\Gamma_5D_\mathrm{W}\Gamma_5=D_\mathrm{W}^\dagger$.

The dispersion relation for free fermion can be obtained from Eq. (3) by taking $U_\mu=1$ (or equivalently $g=0$) and substituting the Fourier transform, $q(n)=\int_{-\pi/a}^{\pi/a}\frac{\mathrm{d}^4p}{(2\pi)^4}\mathrm{e}^{\mathrm{i}p_\mu n_\mu}q(p)$. This leads to $S_\mathrm{F}^{(\mathrm{free})}=\int\frac{\mathrm{d}^4p}{(2\pi)^4}\bar q(-p)\mathcal{G}_\mathrm{F}^{-1}q(p)$ with the free fermion propagator, $\mathcal{G}_\mathrm{F}(p)=(-\mathrm{i}\sum_\mu\bar p_\mu\Gamma_\mu+m(p))/(\sum_\mu\bar p_\mu^2+m^2(p))$, where $\bar p_\mu=\frac{1}{a}\sin(p_\mu a)$, $m(p)=m(0)+\frac{r}{a}\sum_\mu(1-\cos(p_\mu a))$. Since $\sin(p_\mu a)$ becomes zero for $p_\mu a=(0,0,0,0)$, $(\pi,0,0,0)$, $(0,\pi,\pi,\pi)$, (π,π,π,π), there arise $2^4=16$ degenerate fermions if we take $r=0$. This is called the fermion doubling problem on the lattice. In fact, there is a no-go theorem by Nielsen and Ninomiya [7]: The fermion doubling always exists, if the free fermion action on the lattice has (i) bilinearity in quark field, (ii) translational invariance, (iii) hermiticity (in the Minkowski spacetime), (iv) locality in spacetime, and (v) exact chiral symmetry. Indeed, (i)–(v) are all satisfied for $r=0$. In general, $r\neq 0$ leads to a mass splitting of 16 fermions: $m(p)\simeq m(0)$ ($^\forall p_\mu\to 0$) and $m(p)=m(0)+\frac{2r}{a}N_\pi$ ($^\exists p_\mu\to\pi/a$), where $N_\pi(=1,2,3,4)$ being the number of π's in $p_\mu a$. This implies that we can select only one light fermion by choosing $m(0)\simeq 0$ and all the other 15 fermions have masses of $O(1/a)$ for positive r. A price to pay is that the non-vanishing r breaks chiral symmetry explicitly for finite a, i.e., $\{\gamma_5,D_\mathrm{W}\}\neq 0$

even for $m(0) = 0$. Namely, the Nielsen-Ninomiya's no-go theorem is evaded by breaking the condition (v).

Better way to evade the no-go theorem is to break the condition (v) in a way that the definition of chiral symmetry is modified. Suppose we consider a modified chiral rotation in the flavor space, $q \to \mathrm{e}^{-\mathrm{i}\theta_\mathrm{A}\hat{\Gamma}_5}q$, $\bar{q} \to \bar{q}\mathrm{e}^{-\mathrm{i}\theta_\mathrm{A}\Gamma_5}$ with $\hat{\Gamma}_5 = \Gamma_5(1 - 2aD_\mathrm{GW})$, which reduces to the standard axial rotation for $a \to 0$. Here D_GW is a generalized Dirac operator which is constructed so that $\bar{q}D_\mathrm{GW}q$ is invariant under the above transformation even for finite a; $\Gamma_5 D_\mathrm{GW} + D_\mathrm{GW}\hat{\Gamma}_5 = 0$, or equivalently $\{\Gamma_5, D_\mathrm{GW}\} = 2aD_\mathrm{GW}\Gamma_5 D_\mathrm{GW}$. This is called the Ginsparg-Wilson relation [8]. An explicit form of D_GW may be constructed as $D_\mathrm{GW} = \frac{1}{2a}(1 + X/\sqrt{X^\dagger X})$ with $X \equiv D_\mathrm{W}^{(r=1)} - m_0$, where $m_0 a$ being a dimensionless parameter of $O(1)$. Unlike the case of m in the Wilson fermion, m_0 is not directly related to the physical fermion mass. Nevertheless, if we choose the region $0 < m_0 a < 2$, there exists an exact massless mode for $N_\pi = 0$ for finite a, and other 15 modes have a large mass $(2/a)(2N_\pi - m_0 a) > 0$.

The Wilson's fermion action, Eq. (3), can be conveniently rewritten as

$$S_\mathrm{F} = \sum_{n',n} \bar{\psi}(n')F(n',n;U)\psi(n),$$

with

$$F(n',n;U) = \delta_{n'n} - \kappa \sum_{\pm\mu} \delta_{n',n+\hat{\mu}}(r + \Gamma_\mu)U_\mu(n), \qquad (5)$$

where we have redefined the quark field as $\psi = a^{3/2}q/\sqrt{2\kappa}$ with $\kappa = [2(ma+4r)]^{-1}$ being the hopping parameter. If the quark mass m is large, κ is small and the "hopping" to the neighboring lattice site is suppressed.

The functional integration over quarks and gluons in continuum QCD is now transformed to the integration over quarks on each site and gluons on each link in lattice QCD. With Eq. (2) and Eq. (5), the partition function reads

$$\mathcal{Z} = \int [\mathrm{d}U \mathrm{d}\bar{\psi}\mathrm{d}\psi]\mathrm{e}^{-S_\mathrm{G}(U) - S_\mathrm{F}(\bar{\psi},\psi,U)}$$
$$= \int [\mathrm{d}U]\mathrm{Det}\ F(U)\mathrm{e}^{-S_\mathrm{G}(U)} = \int [\mathrm{d}U]\mathrm{e}^{-S_\mathrm{eff}(U)}, \qquad (6)$$

where $S_\mathrm{eff}(U) \equiv S_\mathrm{G}(U) - \mathrm{lnDet}F(U)$. The integration over the group element $[\mathrm{d}U] = \prod_{\mu,n} \mathrm{d}U_\mu(n)$ can be defined through the Haar measure $\mathrm{d}U$ which has the property, $\mathrm{d}(V_\mathrm{L}UV_\mathrm{R}^\dagger) = \mathrm{d}U$ with $V_\mathrm{L,R}$ being arbitrary group elements. Such a measure is unique for compact groups such as SU(N).

Similar to the statistical systems such as the Ising model, observables are obtained by averaging over the statistical weight as $\langle\mathcal{O}\rangle = \frac{1}{\mathcal{Z}}\int [\mathrm{d}U]\mathcal{O}(U)\mathrm{e}^{-S_\mathrm{eff}(U)}$. Some useful observables are shown in Fig. 1: (a) and (b) correspond to the mesic and baryonic correlations, respectively, while (c) is a correlation related to the baryon-baryon interactions. The filled circles are the spacetime points where the quarks and anti-quarks are created or absorbed. Each line with arrow indicates the quark propagator $F^{-1}(n,n';U)$ connecting two spacetime points n and n'. Thus, the explicit forms of the mesic and baryonic correlations are

$$C_\mathrm{M}(n,n') = \frac{1}{\mathcal{Z}}\int [\mathrm{d}U]F^{-1}_{\alpha\beta}(n,n';U)F^{-1}_{\beta\alpha}(n',n;U)\mathrm{e}^{-S_\mathrm{eff}(U)}, \qquad (7)$$

$$C_\mathrm{B}(n,n') = \frac{1}{\mathcal{Z}}\int [\mathrm{d}U]\epsilon_{\alpha\beta\gamma}\epsilon_{\alpha'\beta'\gamma'}F^{-1}_{\alpha\alpha'}(n,n';U)F^{-1}_{\beta\beta'}(n,n';U)F^{-1}_{\gamma\gamma'}(n,n';U)\mathrm{e}^{-S_\mathrm{eff}(U)}, \qquad (8)$$

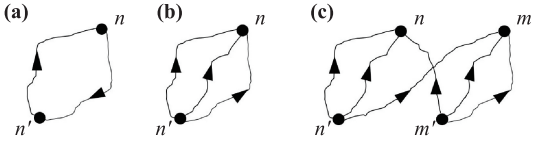

Fig. 1 **(a)** Single meson correlation representing the propagation of a meson created at point n' and absorbed at point n. **(b)** Single baryonic correlation representing the propagation of a baryon created at point n' and absorbed at point n. **(c)** Two baryon correlation which contains the information on baryon-baryon interaction. Reproduced from Ref. [4].

where all the color indices are contracted so that C_M and C_B are gauge invariant. Spacetime, spin and flavor dependences of $C_\mathrm{M}(n,n')$ in (a) and $C_\mathrm{B}(n,n')$ in (b) have all the information on the hadronic states in various different channels, while $C_\mathrm{BB}(n,m,n',m')$ in (c) has the information on baryon-baryon interactions.

3 Lattice QCD: Numerical methods

Suppose we have a lattice having N_s (N_τ) number of sites in each spatial (temporal) direction. Then the total number of links is $N_\mathrm{s}^3 \times N_\tau \times 4$, so that the total number of gluon integrations $\int [\mathrm{d}U]$ for a lattice size $N_\mathrm{s} = N_\tau = 96$ becomes $(N_\mathrm{s}^3 \times N_\tau \times 4)_\mathrm{links} \times 8_\mathrm{color} \sim 3 \times 10^9$. This is hopelessly a large number for standard methods of numerical integration. In this case, the Monte Carlo (MC) integration supplemented by the importance sampling, which is a statistical way to evaluate the integral, plays a powerful role. Most widely used method for generat-

ing configurations in LQCD is the hybrid Monte Carlo (HMC) method [9] and its variations.

The basic procedure of the HMC can be summarized as follows: First, we rewrite the partition function by introducing a conjugate momentum field π, so that $\mathcal{Z}$ is transformed to a phase space functional integral,

$$\mathcal{Z} = \int [\mathrm{d}\phi] \mathrm{e}^{-S(\phi)} = \int [\mathrm{d}\Phi] \mathrm{e}^{-H(\Phi)},$$
$$H(\Phi) = \frac{1}{2}\pi^2 + S(\phi), \tag{9}$$

where $\Phi \equiv (\phi, \pi)$ and $[\mathrm{d}\Phi] \equiv [\mathrm{d}\phi \mathrm{d}\pi]$. Then we follow the steps below:

1) Start with arbitrary chosen initial configuration, ϕ.

2) Generate π with the Gaussian distribution, $P_{\mathrm{G}}(\pi) \propto \exp(-\pi^2/2)$.

3) Evolve Φ under P_{H} with the reversibility condition, $P_{\mathrm{H}}(\Phi \to \Phi') = P_{\mathrm{H}}(\Phi'_r \to \Phi_r)$ with $\Phi_r \equiv (\phi, -\pi)$.

4) Accept the configuration Φ' with the probability, $P_{\mathrm{A}}(\Phi \to \Phi') = \min\{1, \mathrm{e}^{-\Delta H}\}$, where $\Delta H = H(\Phi') - H(\Phi)$. This is called the Metropolis test [10].

5) If the new configuration Φ' is accepted, go to Step 2 with ϕ'. Otherwise, keep the original ϕ and go to Step 2.

The above procedure satisfies the detail balance in phase space, $\mathrm{e}^{-H(\Phi)} P_{\mathrm{A}}(\Phi \to \Phi') = \mathrm{e}^{-H(\Phi')} P_{\mathrm{A}}(\Phi' \to \Phi)$, which leads to the correct weight factor, $W_{\mathrm{eq}}(\Phi) = \mathrm{e}^{-H(\Phi)}$. In practice, the deterministic procedure based on the Molecular Dynamics (MD) evolution along the "computer" time s is useful:

$$\frac{\mathrm{d}}{\mathrm{d}s}\begin{pmatrix}\phi\\ \pi\end{pmatrix} = \begin{pmatrix}0 & 1\\ -1 & 0\end{pmatrix}\begin{pmatrix}\delta H(\phi,\pi)/\delta\phi\\ \delta H(\phi,\pi)/\delta\pi\end{pmatrix} = \begin{pmatrix}\pi\\ -\delta S(\phi)/\delta\phi\end{pmatrix}. \tag{10}$$

This leads to $P_{\mathrm{H}}(\Phi \to \Phi') = \delta(\Phi' - \Phi(s))$, on the phase space trajectories, $\Phi = \Phi(0) \to \Phi(s)$. MD is a nice way to evolve the whole variables on the lattice at once. The computer time s needs to be discretized with a step size ε, which brings inevitable numerical error in MD. However, the Metropolis test in Step 4 eliminates such error so that no extrapolation to $\varepsilon = 0$ is required in HMC. There are numerical algorithms in MD to satisfy the reversibility and preserve the phase space area exactly for finite ε. The leapfrog integrator is one of such algorithms widely used in LQCD. Since it conserves the Hamiltonian with $0(\varepsilon^2)$ accuracy, the acceptance rate in Step 4 can be kept high.

In LQCD simulations, we need to treat the special unitary matrices $U_\mu(n)$ as dynamical variables, i.e., the MD should be performed on the SU(N_c) group manifold. The appropriate choice of the conjugate momentum would be the element of the Lie algebra, $P_l = R_l^a t^a = -\mathrm{i}(\mathrm{d}U_l/\mathrm{d}s)U_l^{-1}$ where we have abbreviated the link index n and site index μ as l for simplicity. This leads to the equation of motion for U_l, i.e., $\mathrm{d}U_l/\mathrm{d}s = \mathrm{i}P_l U_l$. The effective Hamiltonian is naturally written as $H = \mathrm{tr}\sum_l P_l^2 + S_{\mathrm{eff}}(U)$. Then the time-parameter independence $\mathrm{d}H/\mathrm{d}s = 0$ leads to the equation of motion, $\mathrm{d}P_l/\mathrm{d}s = -\mathrm{i}\sum_{i,j} t^a (t^a U_l)_{ij} \partial S_{\mathrm{eff}}(U)/\partial (U_l)_{ij}$. In the actual simulations, the $\ln \mathrm{Det}\ F(U)$ part of the effective action is treated by introducing a set of bosonic variables (pseudofermions) through the identity, $\mathrm{Det}\ F = (\mathrm{Det}\ F^{-1})^{-1} = \int [\mathrm{d}\chi^* \mathrm{d}\chi] \exp\left(-\sum_{IJ} \chi_I^* F_{IJ}^{-1} \chi_J\right)$, where I and J stand for all possible internal and spacetime indices carried by F. For further details of HMC (and its variations) with pseudofermions, see the review [11].

There are two kinds of errors in the data obtained from LQCD simulations. (i) Systematic errors: They are related to the lattice spacing a, the lattice volume L^3, and the quark masses m. During the continuum extrapolation ($a \to 0$) and the thermodynamic extrapolation ($L \to \infty$) under the guidance of the asymptotic scaling for small a and the finite size scaling for large L, some systematic errors are brought in. (ii) Statistical error: It originates from the importance sampling. A very useful procedure to estimate the statistical error commonly used in LQCD is the jackknife resampling method. For example, consider the mean and the unbiased variance of a certain quantity $\mathcal{O}$,

$$\langle \mathcal{O} \rangle = \frac{1}{N}\sum_{n=1}^{N} \mathcal{O}^{(n)} \pm \sqrt{\frac{\sigma^2(\mathcal{O})}{N}},$$
$$\sigma^2(\mathcal{O}) = \left(\frac{N}{N-1}\right)\frac{1}{N}\sum_{n=1}^{N} (\mathcal{O}^{(n)} - \langle \mathcal{O} \rangle)^2, \tag{11}$$

where the factor $\frac{N}{N-1}$ is called the Bessel's correction. The jackknife samples are obtained by $\mathcal{O}_J^{(n)} = \frac{1}{N-1}\sum_{n' \neq n} \mathcal{O}^{(n')}$ with $n = 1, \cdots, N$. If we need to make a quick estimate of the mean and the variance of a function $f(\mathcal{O})$, we have

$$\langle f(\mathcal{O}_J) \rangle = \frac{1}{N}\sum_{n=1}^{N} f(\mathcal{O}_J^{(n)}) \pm \sqrt{\frac{\sigma_J^2(f)}{N}},$$
$$\sigma_J^2(f) = (N-1)\sum_{n=1}^{N} (f(\mathcal{O}_J^{(n)}) - \langle f(\mathcal{O}_J) \rangle)^2. \tag{12}$$

For $f(\mathcal{O}) = \mathcal{O}$, we recover the original mean and variance; $\langle \mathcal{O}_J \rangle = \langle \mathcal{O} \rangle$ and $\sigma_J^2(\mathcal{O}) = \sigma^2(\mathcal{O})$. One can generalize this procedure by dividing N into $N_b = N/n_b$ with the bin-size n_b and create the N_b jackknife samples.

4 Light hadron masses

Meson and baryon masses can be calculated with high accuracy by LQCD simulations with dynamical quarks.

The starting point is the hadronic correlation functions $C_{\rm H=M,B}(n,n')$ in Eqs. (7) and (8) integrated over the spatial coordinates, $\boldsymbol{n}$ and $\boldsymbol{n}'$,

$$C_{\rm H}(\tau)=\sum_{\boldsymbol{n},\boldsymbol{n}'}C_{\rm H}(n,n')\xrightarrow[\tau\to\infty]{}|Z_{\rm H}|^2{\rm e}^{-M_{\rm H}\tau}, \tag{13}$$

where $\tau=(n_4-n_4')a$ is the temporal distance between the source at n' and the sink at n, and $M_{\rm H}$ ($Z_{\rm H}$) corresponds to the mass (the pole residue) of a lightest bound state in each channel. If the temporal extent of the lattice is infinite, one can extract the hadron mass from the formula, $M_{\rm H}=-(1/\tau)\ln C_{\rm H}(\tau)|_{\tau\to\infty}$. In practice, the effective mass defined below is more useful, $aM_{\rm H}^{\rm eff}(\tau)=\ln(C_{\rm H}(\tau)/C_{\rm H}(\tau+a))$. The asymptotic plateau of the effective mass at large τ corresponds to the hadron mass. In actual simulations, the temporal extent is limited ($0\le\tau/a\le N_\tau$), so that the exponential damping of Eq. (13) is replaced by $C_{\rm H}\to\exp[-M_{\rm H}\tau]\pm\exp[-M_{\rm H}(N_\tau a-\tau)]$ where $+(-)$ for the periodic (anti-periodic) boundary condition.

Shown in the left panel of Fig. 2 is the M_π^2-dependence of the N and Ω masses for three different values of a [12]. The crosses are the values extrapolated to the continuum limit and to the physical pion mass. The N and Ω masses predicted from LQCD and corresponding experimental numbers are

$$M_N^{\rm LQCD}=0.936(25)(22)\ {\rm GeV},$$
$$M_\Omega^{\rm LQCD}=1.676(20)(15)\ {\rm GeV}, \tag{14}$$
$$M_N^{\rm exp.}=0.939\ {\rm GeV},$$
$$M_\Omega^{\rm exp.}=1.672\ {\rm GeV}. \tag{15}$$

Note that the numbers in the first (second) parenthesis in Eq. (14) represent the statistical (systematic) errors on the last digits. Shown in the right panel of Fig. 2 is the high precision numerical results of the hadron mass splittings obtained by the QCD+QED lattice simulations with dynamical u,d,s,c quarks [13]. The horizontal lines are the experimental values and the grey shaded regions represent the experimental errors. Red dots are the lattice results with their uncertainties denoted by the vertical error bars. The neutron-proton mass differences from numerical simulations and the corresponding experimental numbers are

$$(M_n-M_p)^{\rm LQCD+QED}=\Delta N=1.51(16)(23)\ {\rm MeV}, \tag{16}$$
$$(M_n-M_p)^{\rm exp.}=1.29\ {\rm MeV}. \tag{17}$$

Since all hadrons are composite particles of quarks and gluons, there are numerous excited states [14]. To extract the properties of the excited hadrons from LQCD, the asymptotic form as shown in Eq. (13) is not sufficient, and more sophisticated methods such as the maximal entropy method (MEM) (reviewed in [15]) and the variational method (reviewed in [16]) are necessary.

5 Baryon-baryon interactions

Understanding of the nuclear force from QCD is one of the most challenging problems in nuclear physics. Several high precision phenomenological NN forces have been constructed to reproduce the neutron-proton and proton-proton scattering data (about 4500 data points) with a $\chi^2/{\rm dof}\sim1$. However, they have typically 20–40 fitting parameters: e.g. the CD Bonn potential, AV18 potential and N^{3}LO chiral effective field theory have 38, 40, and 24 parameters, respectively [17]. If one tries to extend these to hyperon-nucleon and hyperon-hyperon interactions, the task becomes extremely tough since the number of parameters increases and the scattering data are scarce. Under this situation, it is highly desirable to study baryon-baryon interactions from first principle LQCD simulations, where all the hadronic interactions are controlled only by the QCD coupling g and the

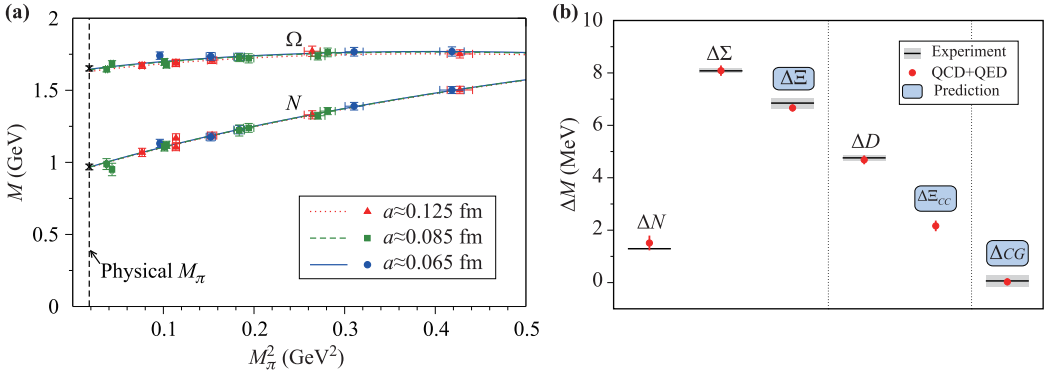

Fig. 2 **(a)** Hadron masses under the changes of the M_π^2 as well as the lattice spacing a [12]. **(b)** Mass splittings in channels that are stable under the strong and electromagnetic interactions. $\Delta N=M_n-M_p$, $\Delta\Sigma=M_{\Sigma^-}-M_{\Sigma^+}$, $\Delta\Xi=M_{\Xi^-}-M_{\Xi^+}$, $\Delta D=M_{D^\pm}-M_{D^0}$, $\Delta\Xi_{cc}=\Delta\Xi_{cc}^{++}-\Delta\Xi_{cc}^{+}$, $\Delta CG=\Delta N-\Delta\Sigma+\Delta\Xi$ [13].

quark mass m whose values are pretty well determined at present by the precision QCD simulations [18].

The finite volume method (FVM), a theoretical framework to study hadron-hadron interactions from LQCD, was first proposed by Lüscher [19]: For two hadrons in a finite box with a spatial size L^3, an exact relation between the energy spectra in the box and the elastic scattering phase shift can be derived. If the range of the hadronic interaction $R_{\rm QCD}$ is sufficiently smaller than the size of the box $R_{\rm QCD} < L/2$, behavior of the equal-time Bethe–Salpeter amplitude (or more precisely the Nambu–Bethe–Salpeter (NBS) amplitude) $\psi(\boldsymbol{r})$ in the interval $R_{\rm QCD} < |\boldsymbol{r}| < L/2$ has sufficient information to relate the phase shift and the energy shift $\Delta E = M_{\rm HH} - 2M_{\rm H}$.

The HAL QCD method was proposed as another theoretical framework to study the hadron-hadron interactions from LQCD by Ishii, Aoki and Hatsuda [3] and was further developed by HAL QCD Collaboration [20]. The starting point is the same equal-time NBS amplitude $\psi(\boldsymbol{r})$: Instead of looking at the amplitude outside the range of the interaction, the internal region $|\boldsymbol{r}| < R_{\rm QCD}$ is considered and an energy-independent non-local potential $U(\boldsymbol{r},\boldsymbol{r}')$ is deduced from $\psi(\boldsymbol{r})$. Since $U(\boldsymbol{r},\boldsymbol{r}')$ in QCD is spatially localized due to the confinement of quarks and gluons, it is affected only weakly by the finite lattice volume. Physical quantities such as the scattering phase shifts, bound state spectra, and resonance energies can be calculated by solving the integro-differential differential equation satisfied by $\psi(\boldsymbol{r})$ with $U(\boldsymbol{r},\boldsymbol{r}')$.

Recently, a detailed comparison between the FVM and the HAL QCD method has been carried out: Although they agree with each other quite accurately for non-resonant pion-pion scattering, large signal to noise ratio inherent in the effective mass $\Delta E^{\rm eff}(\tau)$ for baryon-baryon systems [21] turns out to be a fatal blow for FVM to extract scattering observables [22–24].

5.1 Master equation in HAL QCD method

Let us consider the baryon-baryon correlation in Fig. 1(c) and define the equal-time NBS amplitude $\psi_\ell(\boldsymbol{r},\tau)$ from its large τ behavior:

$$C_{\rm BB}(\boldsymbol{r},\tau) = \sum_{\boldsymbol{n}',\boldsymbol{m}'} C_{\rm BB}(n,m,n',m')|_{n_4=m_4,n_4'=m_4'} \to \sum_\ell a_\ell \psi_\ell(\boldsymbol{r},\tau) {\rm e}^{-E_\ell \tau}, \quad (18)$$

where $\boldsymbol{r} = (\boldsymbol{n}-\boldsymbol{m})a$, $\tau = (n_4 - n_4')a$, and $\psi_\ell(\boldsymbol{r},\tau)$ being the NBS wave function for ℓ-th scattering state on the lattice. For large lattice size, E_ℓ is very dense, so that it is impossible to identify each level. This causes a fatal problem in FVM as mentioned above. On the other hand, if we define $C_{\rm BB}(\boldsymbol{r};\tau) = \mathcal{R}(\boldsymbol{r},\tau){\rm e}^{-2M_{\rm B}\tau}$, the following integro-differential equation can be derived below the inelastic threshold ($\tau > M_\pi^{-1}$),

$$\left\{\frac{1}{4M_{\rm B}}\frac{\partial^2}{\partial\tau^2} - \frac{\partial}{\partial\tau} - H_0\right\}\mathcal{R}(\boldsymbol{r},\tau) = \int {\rm d}^3r' U(\boldsymbol{r},\boldsymbol{r}')\mathcal{R}(\boldsymbol{r}',\tau), \quad (19)$$

with $H_0 = -\nabla^2/M_{\rm B}$. This is the master equation which has the correct information of the S-matrix and hence the scattering phase shift for elastic BB scatterings [20].

If we further focus on the energies much below the inelastic threshold, the velocity expansion of $U(\boldsymbol{r},\boldsymbol{r}')$ in terms of its non-locality can be adopted. In fact, the potential with hermiticity, rotational invariance, parity symmetry, and time-reversal invariance may be expanded as [25]

$$U(\boldsymbol{r},\boldsymbol{r}') = V(\boldsymbol{r},\boldsymbol{v})\delta(\boldsymbol{r}-\boldsymbol{r}')$$

with

$$V(\boldsymbol{r},\boldsymbol{v}) = \underbrace{V_{\rm C}(r) + V_{\rm T}(r)S_{12}}_{\rm LO} + \underbrace{V_{\rm LS}(r)\boldsymbol{L}\cdot\boldsymbol{S}}_{N{\rm LO}} + \underbrace{O(\boldsymbol{v}^2)}_{N^2{\rm LO}} + \cdots, \quad (20)$$

where $\boldsymbol{v} = \boldsymbol{p}/(M_{\rm B}/2)$, $\boldsymbol{L} = \boldsymbol{r}\times\boldsymbol{p}$, $\boldsymbol{p} = -i\nabla$ and $S_{12} = 3(\boldsymbol{\sigma}_1\cdot\boldsymbol{r})(\boldsymbol{\sigma}_2\cdot\boldsymbol{r})/r^2 - \boldsymbol{\sigma}_1\cdot\boldsymbol{\sigma}_2$. The central potential $V_{\rm C}$ and the tensor potential $V_{\rm T}$ are classified as the leading order (LO) potentials since they are of $O(\boldsymbol{v}^0)$. The next-to-leading (NLO) potential of $O(\boldsymbol{v})$ is the spin-orbit potential $V_{\rm LS}(r)$.

5.2 Nearly physical point simulations

By using the 11 PFlops supercomputer K at RIKEN Center for Computational Science, $(2+1)$-flavor gauge configurations on the 96^4 lattice are generated with the Iwasaki gauge action at $\beta = 1.82$ and nonperturbatively $\mathcal{O}(a)$-improved Wilson quark action with stout smearing [27, 28]. The lattice spacing is $a \simeq 0.0846$ fm ($a^{-1} \simeq 2.333$ GeV) and the pion mass, the kaon mass and the nucleon masses are $m_\pi \simeq 146$ MeV, $m_K \simeq 525$ MeV and $m_N \simeq 964$ MeV, respectively. (These masses are higher than the physical values by about 8%, 6% and 3%, respectively, due to slightly larger quark masses at the simulation point.) The lattice size, $La \simeq 8.1$ fm, is sufficiently large to accommodate two baryons in a box. We employ the wall quark source with the Coulomb gauge fixing, and the periodic (Dirichlet) boundary condition is used for spatial (temporal) directions.

5.3 Two-body potentials in irreducible flavor basis

Shown in Fig. 3 are the S-wave interaction between octet baryons in the flavor irreducible basis:

$$\mathbf{8}\otimes\mathbf{8} = (\mathbf{27}\oplus\mathbf{8}_s\oplus\mathbf{1})_{\rm sym.}\oplus(\mathbf{10}^*\oplus\mathbf{10}\oplus\mathbf{8}_a)_{\rm anti-sym.}, \quad (21)$$

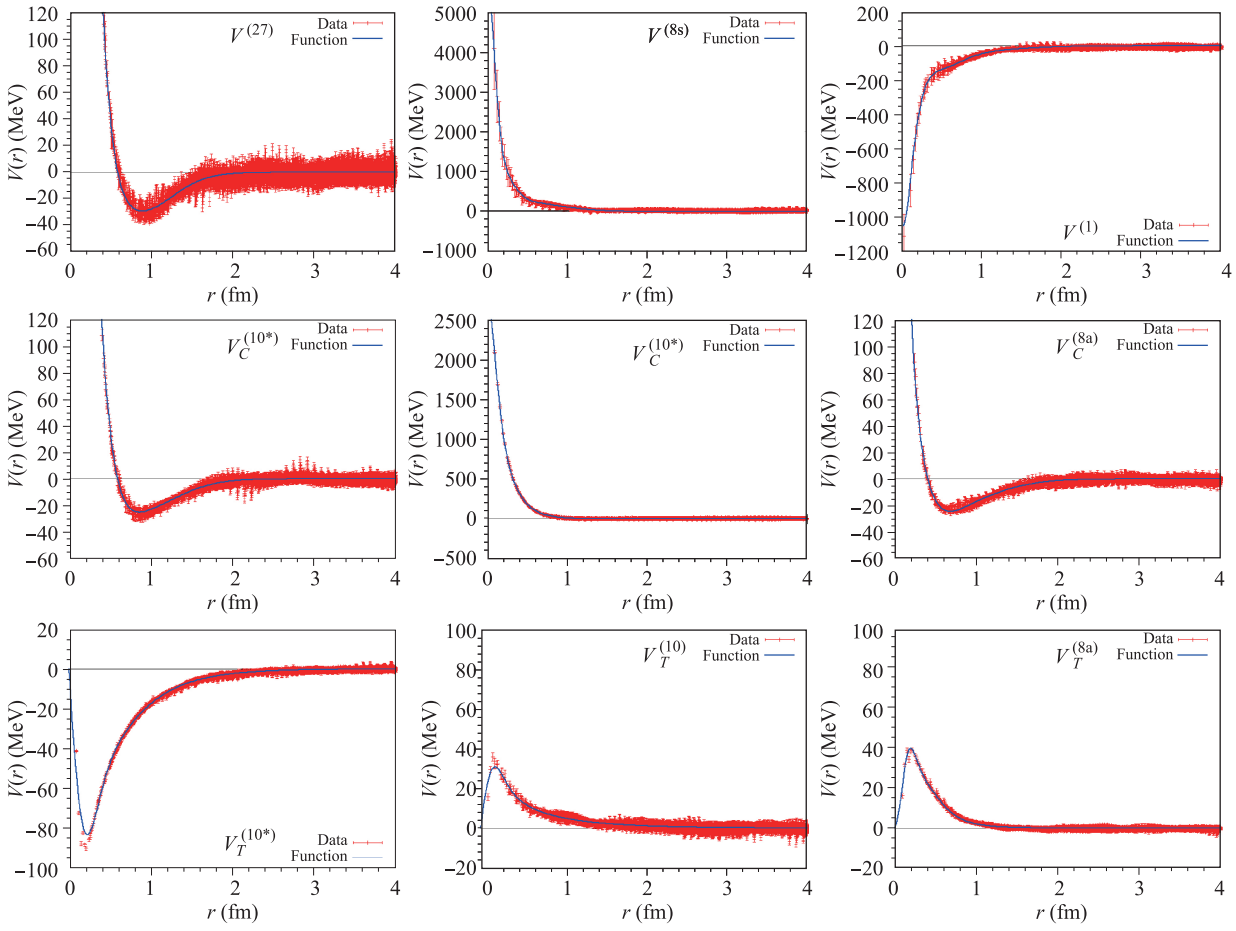

Fig. 3 Potential of baryon-baryon S-wave interactions in the irreducible flavor basis, which are obtained by rotating data of hyperon interaction potentials in strangeness $S = -2$ sector [5].

where "sym." and "anti-sym." stand for the flavor symmetry under the exchange of two baryons. For orbital S-wave, the Pauli principle between two baryons imposes **27**, $\mathbf{8}_s$ and **1** to be spin singlet ($^1S_0$) while $\mathbf{10}^*$, **10** and $\mathbf{8}_a$ to be spin triplet ($^3S_1$). Then one may define the potential in each channel as

$$
\begin{aligned}
&^1S_0 : V^{(\mathbf{27})}(r), V^{(\mathbf{8}_s)}(r), V^{(\mathbf{1})}(r), \\
&^3S_1 : V^{(\mathbf{10}^*)}(r), V^{(\mathbf{10})}(r), V^{(\mathbf{8}_a)}(r).
\end{aligned} \tag{22}
$$

• The upper left panel of Fig. 3 is the central potential $V^{(\mathbf{27})}(r)$ to which the $^1S_0$ nucleon-nucleon potential belongs. It has a repulsive core at short distance and an attractive pocket at intermediate distance.

• As shown in the upper right panel of Fig. 3, the structure of the potential is quite different for $V^{(\mathbf{1})}(r)$ to which the flavor singlet H dibaryon (composed of $uuddss$) belongs. There is no repulsive core and the attraction increases as the pion mass decreases.

• The middle left and lower left panels of Fig. 3 are the central potential and the tensor potential of $V^{(\mathbf{10}^*)}(r)$, respectively. The $^3S_1$ nucleon-nucleon potential belongs to this channel. The central part has a similar structure as the $^1S_0$ channel, while the tensor part has rather strong attraction with the longest range. The latter aspect is qualitatively consistent with the one-pion-exchange picture.

5.4 Di-omega: The most strange dibaryon

So far, only one stable dibaryon, the deuteron, has been observed experimentally. It is a loosely bound system of the proton and the neutron in spin-triplet and isospin-singlet channel. In recent years, there are renewed experimental interests in the dibaryons due to exclusive measurements in hadron reactions [29] as well as the direct measurement in relativistic heavy-ion collisions [30].

All the members of **8** are stable under strong decay. This is why the forces between octet baryons in $\mathbf{8} \otimes \mathbf{8}$ are most relevant in the physics of hypernuclei and of neutron stars. Also, the elusive H-dibaryon (a combination of $\Lambda\Lambda$, $N\Xi$ and $\Sigma\Sigma$) is in this representation [31] and does not suffer from the Pauli exclusion principle in the flavor-SU(3) limit. On the other hand, only Ω in **10**

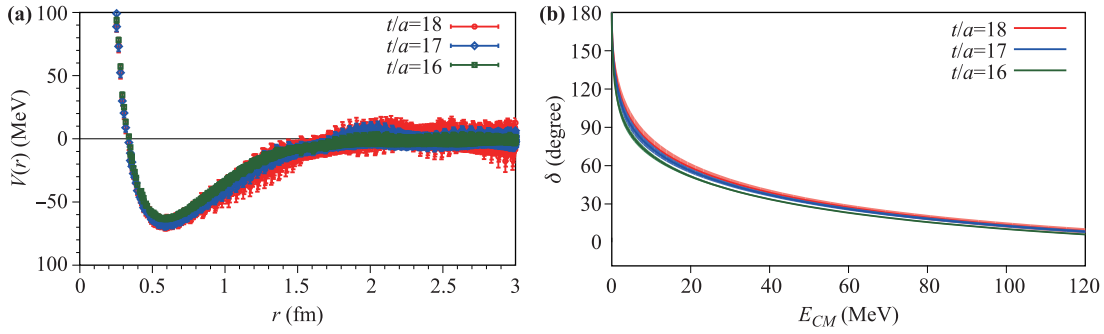

Fig. 4 **(a)** The ΩΩ potential $V(r)$ in the $^1S_0$ channel at Euclidean time $t/a = 16, 17$, and 18 [6]. **(b)** The ΩΩ phase shift $\delta(k)$ in the $^1S_0$ channel as a function of the center of mass kinetic energy $E_{\rm CM} = 2\sqrt{k^2 + m_\Omega^2} - 2m_\Omega$ [6].

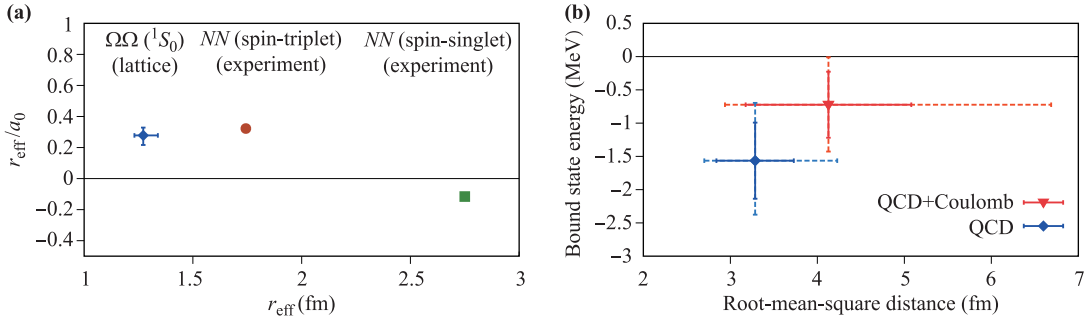

Fig. 5 **(a)** The dimensionless ratio of the effective range $r_{\rm eff}$ and the scattering length a_0 as a function of $r_{\rm eff}$ for di-Omega in the $^1S_0$ channel as well as for the spin-triplet NN system (the deuteron channel) and for the spin-singlet NN system (the neutron-neutron channel). **(b)** Bound state energy of the di-Omega and the root-mean-square distance between Ωs obtained from the potential. Filled diamond (triangle) corresponds to the result at $t/a = 17$ without (with) the Coulomb repulsion. The statistical errors are shown by the solid lines, while the systematic errors estimated from the difference between the data at $t/a = 17$ and those at $t/a = 16, 18$ are shown by the dashed lines. Reproduced from Ref. [6].

is stable under strong decay. Therefore, in the $\mathbf{8} \otimes \mathbf{10}$ representation, the most promising candidate of stable dibaryon is $N\Omega$ [32]. The Pauli exclusion principle does not work in this case too, so that there is a possibility to have a bound state in the S-wave and total-spin 2 channel [33]. Such a system is indeed studied by the two-particle momentum correlation in high-energy heavy-ion collisions both theoretically and experimentally [34].

In the decuplet-decuplet channnel, we have

$$\mathbf{10} \otimes \mathbf{10} = (\mathbf{28} \oplus \mathbf{27})_{sym.} \oplus (\mathbf{35} \oplus \mathbf{10}^*)_{anti\text{-}sym.}. \quad (23)$$

Only possible stable state under strong decay is the ΩΩ system in the symmetric **28** representation. Again, the quark Pauli principle does not operate in this channel [35]. Note that the celebrated ABC resonance (ΔΔ in the spin-3 and isospin-0 channel) [29, 36] belongs to the anti-symmetric $\mathbf{10}^*$ representation, while ΔΔ in the spin-0 and isospin-3 channel is in the same multiplet with ΩΩ. The ΩΩ interaction at low energies has been investigated so far by using phenomenological quark models [37–40].

Under this situation, the di-omega (the ΩΩ system) in the $^1S_0$ channel (the most strange dibaryon) has been studied on the basis of the (2+1)-flavor lattice QCD simulations with a large volume $(8.1\ {\rm fm})^3$ and nearly physical pion mass $m_\pi \simeq 146$ MeV at a lattice spacing $a \simeq 0.0846$ fm [6]. The $^1S_0$ potential $V(r)$ obtained from Eq. (19) with the lattice measurement of $R(\boldsymbol{r}, t)$ is shown in Fig. 4(a) for $t/a = 16, 17$, and 18. The statistical errors for $V(r)$ at each r are estimated by the jackknife method with the bin size of 40 configurations. We observe that the potentials at $t/a = 16, 17$, and 18 are nearly identical within statistical errors as expected from the time-dependent HAL QCD method [20]. The di-omega potential $V(r)$ has qualitative features similar to the central potential of the nucleon-nucleon (NN) interaction, i.e., the short range repulsion and the intermediate range attraction. There are, however, two quantitative differences: (i) the short range repulsion is much weaker in the di-omega case possibly due to the absence of quark Pauli exclusion effect, and (ii) the attractive part is much short-ranged due to the absence of pion exchanges.

We fit $V(r)$ in Fig. 4(a) in the range $r = 0 - 6$ fm by three Gaussians, and calculate the ΩΩ scattering phase shifts $\delta(k)$ in the $^1S_0$ channel as shown in Fig. 4(b) as a function of the kinetic energy in the center of mass frame,

$E_{\rm CM} = 2\sqrt{k^2 + m_\Omega^2} - 2m_\Omega$. The error bands reflect the statistical uncertainty of the potential in Fig. 4. All three cases show that $\delta(0)$ starts from 180°, which indicates the existence of a bound $\Omega\Omega$ system.

The scattering length a_0 and the effective range $r_{\rm eff}$ in the $^1S_0$ channel is extracted from $\delta(k)$ through the effective range expansion, $k\cot\delta(k) = -\frac{1}{a_0} + \frac{1}{2}r_{\rm eff}k^2 + \cdots$, with the sign convention of nuclear and atomic physics:

$$a_0^{(\Omega\Omega)} = 4.6(6)(^{+1.2}_{-0.5})\ \text{fm}, \quad r_{\rm eff}^{(\Omega\Omega)} = 1.27(3)(^{+0.06}_{-0.03})\ \text{fm}. \tag{24}$$

In Fig. 5(a), the dimensionless ratios, $r_{\rm eff}/a_0$ as a function of $r_{\rm eff}$ are plotted for the $\Omega\Omega$ system in the $^1S_0$ channel as well as those for the spin-triplet NN system (the deuteron channel) and for the spin-singlet NN system (the neutron-neutron channel). Shown in Fig. 5(b) is the bound state energy and the root-mean-square distance ($\sqrt{\langle r^2\rangle}$) of the $\Omega\Omega$ bound state obtained from the potential. The binding energy without Coulomb repulsion shown by the blue diamond in Fig. 5(b), $B_{\Omega\Omega}^{(\rm QCD)} = 1.6(6)(^{+0.7}_{-0.6})$ MeV, is consistent with the value obtained from the general formula for loosely bound states [41]; $B_{\Omega\Omega} = \frac{1}{m_\Omega r_{\rm eff}^2}\left(1 - \sqrt{1 - \frac{2r_{\rm eff}}{a_0}}\right)^2 \simeq 1.5$ MeV. Associated with this small binding energy, $\sqrt{\langle r^2\rangle}$ is as large as 3–4 fm which is consistent with the expectation, $\sqrt{\langle r^2\rangle} \sim a_0$, for loosely bound states. The Coulomb repulsion can be evaluated by adding α/r with $\alpha = e^2/(4\pi)$ to the potential obtained from lattice QCD, i.e., $V^{(\rm QCD+Coulomb)} \equiv V^{(\rm QCD)} + \alpha/r$. This reduces the above binding energy by a factor of two, $B_{\Omega\Omega}^{(\rm QCD+Coulomb)} = 0.7(5)(5)$ MeV as shown in Fig. 5(b) by the red triangle.

The small binding energy $B_{\Omega\Omega}$ as well as the large scattering length $a_0^{(\Omega\Omega)}$ are the natural consequence of the large cancellation between the long-range attraction and the short-range repulsion of $V(r)$, a situation common in nuclear and atomic physics. Although $V(r)$ is not a direct observable, it provides an important intermediate step to link the QCD scale (GeV) to nuclear physics scale (MeV), since it is hopeless to measure the binding energy directly from lattice QCD using the FVM for large lattice volumes and physical quark masses [24].

From the phenomenological point of view, such a system can be best searched by the measurement of pair-momentum correlation $C(Q)$ with Q being the relative momentum between two baryons produced in relativistic heavy-ion collisions [30]. Experimentally, each Ω can be identified through a successive weak decay, $\Omega^- \to \Lambda + K^- \to p + \pi^- + K^-$. Note that a large scattering length is the important element for $C(Q)$ to have characteristic enhancement at small relative momentum Q. Moreover, the effect of the Coulomb interaction can be effectively eliminated by taking a ratio of $C(Q)$ between small and large collision systems [34].

6 Summary

Lattice QCD for single-hadron has reached the level of precision science with an accuracy of $O(1\%)$. Moreover, the multi-hadron, in particular the two-baryon systems, can be studied with nearly physical quark masses on a large lattice box. This enables us to make a solid connection between the fundamental laws of strong interaction (QCD) and the many-baryon systems (atomic nuclei and neutron stars). Simultaneous developments of theoretical frameworks, fast numerical algorithms and the fast supercomputers turn out to be crucial for such progress. Lattice QCD is now used to make theoretical predictions for future experiments in nuclear physics: Weakly bound di-Omega predicted by HAL QCD Collaboration is a first example of such prediction.

Acknowledgements I would like to dedicate this article to Prof. Akito Arima who has made fundamental contributions to modern nuclear physics.

References

1. K. G. Wilson, Confinement of quarks, *Phys. Rev. D* 10(8), 2445 (1974)
2. A. Ukawa, Kenneth Wilson and lattice QCD, *J. Stat. Phys.* 160(5), 1081 (2015)
3. N. Ishii, S. Aoki, and T. Hatsuda, Nuclear force from lattice QCD, *Phys. Rev. Lett.* 99(2), 022001 (2007)
4. T. Hatsuda, Lattice quantum chromodynamics, *Lect. Notes Phys.* 936, 55 (2017)
5. T. Inoue, et al. (HAL QCD Collaboration), Hyperon single-particle potentials from QCD on lattice, *PoS INPC* 2016, 277 (2016)
6. S. Gongyo, K. Sasaki, S. Aoki, T. Doi, T. Hatsuda, Y. Ikeda, T. Inoue, T. Iritani, N. Ishii, T. Miyamoto, and H. Nemura, Most strange dibaryon from lattice QCD, *Phys. Rev. Lett.* 120(21), 212001 (2018)
7. H. B. Nielsen and M. Ninomiya, A no-go theorem for regularizing chiral fermions, *Phys. Lett.* 105(2–3), 219 (1981)
8. P. H. Ginsparg and K. G. Wilson, A remnant of chiral symmetry on the lattice, *Phys. Rev. D* 25(10), 2649 (1982)
9. S. Duane, A. D. Kennedy, B. J. Pendleton, and D. Roweth, Hybrid Monte Carlo, *Phys. Lett. B* 195(2), 216 (1987)
10. N. Metropolis, A. W. Rosenbluth, M. N. Rosenbluth, A. H. Teller, and E. Teller, Equation of state calculations by fast computing machines, *J. Chem. Phys.* 21(6), 1087 (1953)

11. S. Schaefer, Status and challenges of simulations with dynamical fermions, *PoS LATTICE* 2012, 001 (2012)
12. S. Durr, Z. Fodor, J. Frison, C. Hoelbling, R. Hoffmann, S. D. Katz, S. Krieg, T. Kurth, L. Lellouch, T. Lippert, K. K. Szabo, and G. Vulvert, *ab initio* determination of light hadron masses, *Science* 322(5905), 1224 (2008)
13. S. Borsanyi, S. Durr, Z. Fodor, C. Hoelbling, S. D. Katz, S. Krieg, L. Lellouch, T. Lippert, A. Portelli, K. K. Szabo, and B. C. Toth, *ab initio* calculation of the neutron-proton mass difference, *Science* 347(6229), 1452 (2015)
14. The Review of Particle Physics, http://pdg.lbl.gov/ (2015)
15. M. Asakawa, T. Hatsuda, and Y. Nakahara, Maximum entropy analysis of the spectral functions in lattice QCD, *Prog. Part. Nucl. Phys.* 46(2), 459 (2001)
16. Z. Fodor and C. Hoelbling, Light hadron masses from lattice QCD, *Rev. Mod. Phys.* 84(2), 449 (2012)
17. R. Machleidt, Nuclear forces from chiral effective field theory, arXiv: 0704.0807 [nucl-th]
18. S. Aoki, Y. Aoki, C. Bernard, T. Blum, G. Colangelo, et al., Review of lattice results concerning low-energy particle physics, *Eur. Phys. J. C* 74(9), 2890 (2014)
19. M. Lüscher, Two-particle states on a torus and their relation to the scattering matrix, *Nucl. Phys. B* 354(2–3), 531 (1991)
20. N. Ishii, S. Aoki, T. Doi, T. Hatsuda, Y. Ikeda, T. Inoue, K. Murano, H. Nemura, and K. Sasaki (HAL QCD Collaboration), Hadron–hadron interactions from imaginary-time Nambu–Bethe–Salpeter wave function on the lattice, *Phys. Lett. B* 712(4–5), 437 (2012)
21. G. P. Lepage, in: From Actions to Answers: Proceedings of the TASI 1989, edited by T. Degrand and D. Toussaint, World Scientific, Singapore, 1990
22. T. Iritani, T. Doi, S. Aoki, S. Gongyo, T. Hatsuda, Y. Ikeda, T. Inoue, N. Ishii, K. Murano, H. Nemura, and K. Sasaki, Mirage in temporal correlation functions for baryon-baryon interactions in lattice QCD, *JHEP* 1610(10), 101 (2016)
23. T. Iritani, S. Aoki, T. Doi, T. Hatsuda, Y. Ikeda, T. Inoue, N. Ishii, H. Nemura, and K. Sasaki, Are two nucleons bound in lattice QCD for heavy quark masses? Consistency check with Lüscher's finite volume formula, *Phys. Rev. D* 96(3), 034521 (2017)
24. S. Aoki, T. Doi, and T. Iritani, Sanity check for NN bound states in lattice QCD with Lüscher's finite volume formula–Exposing symptoms of fake plateaux, arXiv: 1707.08800 [hep-lat]
25. S. Okubo and R. E. Marshak, Velocity dependence of the two-nucleon interaction, *Ann. Phys.* 4, 166 (1958)
26. T. Inoue, et al. (HAL QCD Collaboration), Equation of state for nucleonic matter and its quark mass dependence from the nuclear force in Lattice QCD, *Phys. Rev. Lett.* 111(11), 112503 (2013)
27. T. Doi, et al., Baryon interactions from lattice QCD with physical masses – Overview and $S = 0, -4$ sectors, *PoS LATTICE* 2016, 110 (2017)
28. K. Sasaki, et al., Baryon interactions from lattice QCD with physical masses – $S = -2$ sector, *PoS LATTICE* 2016, 116 (2017)
29. H. Clement, On the history of dibaryons and their final observation, *Prog. Part. Nucl. Phys.* 93, 195 (2017)
30. S. Cho, et al. (ExHIC Collaboration), Exotic hadrons from heavy ion collisions, *Prog. Part. Nucl. Phys.* 95, 279 (2017)
31. R. L. Jaffe, Perhaps a stable dihyperon, *Phys. Rev. Lett.* 38(5), 195 (1977)
32. T. Goldman, K. Maltman, K. E. Stephenson, K. E. Schmidt, and F. Wang, Strangeness −3 dibaryons, *Phys. Rev. Lett.* 59(6), 627 (1987)
33. F. Etminan, et al. (HAL QCD Collaboration), Spin-2 NW dibaryon from lattice QCD, *Nucl. Phys. A.* 928, 89 (2014)
34. K. Morita, A. Ohnishi, F. Etminan, and T. Hatsuda, Probing multistrange dibaryons with proton-omega correlations in high-energy heavy ion collisions, *Phys. Rev. C* 94(3), 031901 (2016)
35. M. Oka, K. Shimizu, and K. Yazaki, Quark cluster model of Baryon-Baryon interaction, *Prog. Theor. Phys. Suppl.* 137, 1 (2000)
36. F. Dyson and N. H. Xuong, $Y = 2$ states in $SU(6)$ theory, *Phys. Rev. Lett.* 13(26), 815 (1964)
37. Z. Y. Zhang, Y. W. Yu, P. N. Shen, L. R. Dai, A. Faessler, and U. Straub, Hyperon-nucleon interactions in a chiral $SU(3)$ quark model, *Nucl. Phys. A.* 625(1–2), 59 (1997)
38. Z. Y. Zhang, Y. W. Yu, C. R. Ching, T. H. Ho, and Z. D. Lu, Suggesting a di-omega dibaryon search in heavy ion collision experiments, *Phys. Rev. C* 61(6), 065204 (2000)
39. F. Wang, J. L. Ping, G. H. Wu, L. J. Teng, and T. Goldman, Quark delocalization, color screening, and dibaryons, *Phys. Rev. C* 51(6), 3411 (1995)
40. F. Wang, G. H. Wu, L. J. Teng, and T. Goldman, Quark delocalization, color screening, and nuclear intermediate range attraction, *Phys. Rev. Lett.* 69(20), 2901 (1992)
41. P. Naidon and S. Endo, Efimov physics: A review, *Rep. Prog. Phys.* 80(5), 056001 (2017)